Materials and Structures
DOI 10.1617/s11527-006-9207-8

ORIGINAL ARTICLE

Textile-reinforced mortar (TRM) versus FRP as strengthening material of URM walls: in-plane cyclic loading

Catherine G. Papanicolaou · Thanasis C. Triantafillou · Kyriakos Karlos · Myrto Papathanasiou

Received: 10 June 2006 / Accepted: 25 October 2006

Abstract In this study the application of a new structural material, namely textile-reinforced mortar (TRM), as a means of increasing the load carrying capacity and deformability of unreinforced masonry walls subjected to cyclic in-plane loading is experimentally investigated. The application of externally bonded TRM is considered in this work as an alternative method to the application of fiber-reinforced polymers (FRP). Hence, the effectiveness of TRM overlays is evaluated in comparison to the one provided by FRPs. Medium-scale tests were carried out on 22 masonry walls subjected to in-plane cyclic loading. Three types of specimens were used: (a) shear walls; (b) beam-columns; and (c) beams. The parameters under investigation included the matrix material (mortar versus resin), the number of textile layers and the compressive stress level applied to shear walls and beam-columns. Compared with their resin-impregnated counterparts, mortar-impregnated textiles may result in generally lower effectiveness in terms of strength, but in much higher in terms of deformability. From the results obtained in this study it is believed that TRMs hold strong promise as a solution for the structural upgrading of masonry structures under in-plane loading.

Keywords Textiles · Mortars · TRM · FRP · In-plane cyclic loading · Seismic retrofitting

C. G. Papanicolaou (✉) · T. C. Triantafillou · K. Karlos · M. Papathanasiou
Department of Civil Engineering, University of Patras, Patras GR-26500, Greece
e-mail: kpapanic@upatras.gr

1 Introduction and background

A number of drawbacks associated with fiber-reinforced polymers (FRP) as strengthening materials of masonry structures are summarized by the authors in [1]. These drawbacks are attributed mainly to the use of organic binders (resins) and are repeated here for the sake of completeness: (a) poor behavior of resins at temperatures above the glass transition temperature; (b) relatively high cost of epoxies; (c) potential hazards for the manual worker; (d) difficulty to apply FRPs on wet surfaces or at low temperatures; (e) lack of vapor permeability; (f) incompatibility of epoxy resins and some substrate materials (e.g. clay); and (g) difficulty to conduct post-earthquake assessment of the damage suffered by the masonry behind the FRP. In addition, certain properties of clay masonry, such as the porosity and surface unevenness and/or roughness, which affect the epoxy-brick bond behavior, as well as restrictions related to intervention strategies for historic masonry buildings (e.g. requirements for reversibility), may possibly inhibit the success of FRP application.

One possible solution to the above problems would be the replacement of organic binders with inorganic ones, e.g. cement-based mortars. These cementitious composites have a relatively long-term record in structural engineering, especially in the development of thin section products [2], but they fail to ensure the efficient use of continuous fibers, due to poor bond conditions. These conditions could be improved and fiber-matrix interactions could be made tighter when continuous fiber sheets are replaced by textiles. These materials comprise fabric meshes made of long woven, knitted or even unwoven fiber rovings in at least two (typically orthogonal) directions. The density, that is the quantity and the spacing, of rovings in each direction can be controlled independently, thus affecting the mechanical characteristics of the textile and the degree of penetration of the mortar matrix through the mesh openings (which in turn determines the degree of the mechanical interlock achieved).

Although research on the use of textile meshes as reinforcement of cementitious products commenced in the early 1980s, developments in this field progressed rather slowly until the late 1990s. But during the past five years or so, the research community has put a considerable effort on the use of textiles as reinforcement of cement-based products, primarily in new constructions (e.g. [3–7]). In the field of strengthening, textiles combined with mortars were used recently as external reinforcement of concrete: by [8–10] for flexural and shear strengthening; by [11, 12] for shear strengthening; and by [11, 13] for confinement. Finally, textiles combined with mortars were used recently as a means of increasing the strength of masonry, either in diagonal compression [14] or in uniaxial compression through confinement [15, 16].

As described in [1], the authors tested under cyclic loading conditions, for the first time, masonry walls strengthened on both sides with textile-reinforced mortars (TRM), and they compared the efficiency of TRM jackets with their FRP counterparts. Additional comparisons were also made with respect to near-surface mounted (NSM) reinforcement. The authors concluded that TRMs comprise an extremely promising solution for the structural upgrading of masonry walls under out-of-plane loading. The results concerning in-plane loading are presented in the present study.

2 Experimental program

2.1 Scope and method

The main objective of the experimental program was to provide a better understanding on the effectiveness of externally bonded TRM as strengthening materials of unreinforced masonry walls subjected to in-plane cyclic loading. The investigation was carried out on three series of medium-scale, single-wythe, fired clay brick wallettes composed of running bond courses: (a) Series A (shear walls) specimens measured 1,300 mm in height and 800 mm in width (Fig. 1a); (b) Series B (beam-columns) specimens measured 1,300 mm in height and 400 mm in width (Fig. 1b); and (c) Series C (beams) specimens measured 400 mm in height and 1,300 mm in width (Fig. 1c). All specimens were constructed in the laboratory by an experienced mason using perforated bricks (185 × 85 ×

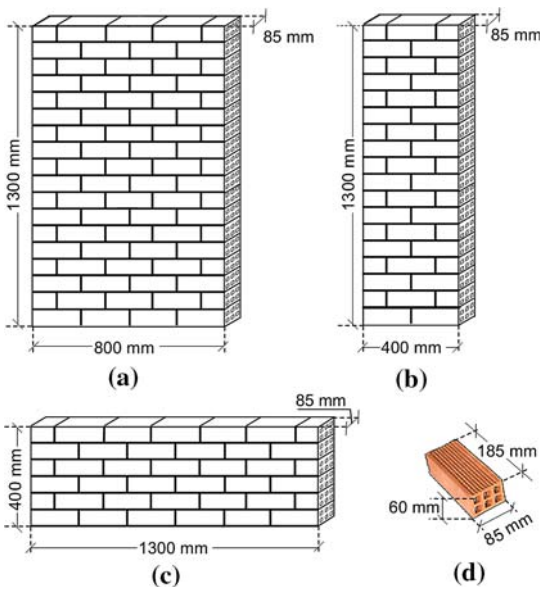

Fig. 1 (**a**) Series A specimens; (**b**) Series B specimens; (**c**) Series C specimens; and (**d**) 6-hole clay bricks

60 mm—Fig. 1d), with the perforations running in parallel to the unit's length. For all walls, the first row of bricks was laid on a 10 mm thick horizontal layer of mortar and all joints (bed and head) were approximately 10 mm thick.

Two major parameters were considered in the investigation, namely the use of inorganic mortar versus resin-based matrix material for the textile reinforcement and the number of textile layers (one or two layers, applied on both sides). Testing of Series A and B specimens aimed to investigate also the effect of the axial compressive load level exerted on the walls simultaneously with the in-plane load applied in the transverse direction. Finally, for Series A specimens only, the effectiveness of near surface mounted carbon-fiber reinforced polymer (CFRP) strips placed along bed slots, in comparison to textiles, was also explored. All specimens, but the control ones of Series B and C, were tested under cyclic in-plane loading.

It is noted that the strengthening schemes applied on wall specimens for the purpose of this study were selected in order to provide useful conclusions on the relative performance of TRM versus FRP jackets and were not necessarily meant to account for realistic fiber quantities, which, in real interventions, could be optimized according to the design requirements.

2.2 Test specimens and materials

All specimens were constructed using ridge-faced, 6-hole, horizontally perforated clay bricks, supplied by a local manufacturer, and a general purpose masonry cement mortar. Series A included six different designs: the control specimen (without strengthening); two specimens each symmetrically (on both sides) strengthened with one or two layers of textile bonded with a commercial polymer-modified cement mortar; their counterparts, in which textiles were bonded with a two-part epoxy adhesive; and a specimen with five NSM CFRP strips per side, placed along slots formed in every third bed joint (starting from the third one from the wall's base). Two identical groups of Series A walls featuring the previously described designs were constructed in order to be tested under different compressive stress levels: a moderate one, at 10% of the wall's compressive strength (perpendicular to the bed joints) and a low one, at 2.5% of the compressive strength.

Both Series B and C included four different designs each: the control specimen (without strengthening); two specimens each symmetrically strengthened with one or two layers of textile bonded with a commercial polymer-modified cement mortar; and one specimen symmetrically strengthened with one layer of textile bonded with a two-part epoxy adhesive. Four specimens of Series B were tested under a moderate compressive stress level, corresponding to 10% of the wall's compressive strength (perpendicular to the bed joints), whereas three additional specimens (the control and two others, each symmetrically strengthened with one or two TRM layers) were tested under a higher compressive stress level, at 25% of the wall's strength. All specimens in Series C were tested without axial loading. A total of 22 specimens were tested.

Specimens are given the notation Y_XN_Z, where Y denotes the specimens' Series (A, B or C), X denotes the type of binder used (M for mortar and R for resin), N denotes the number of layers (1 or 2) and the subscript $_Z$ denotes the axial compressive load level (2.5% or 10% for Series A and 10% or 25% for Series B). The designations C and NSM5 (in place of XN) are used to distinguish the control specimens and the ones receiving five near surface mounted reinforcement strips on each side, respectively. All types of specimens tested in this study are summarized in the first column of Table 1.

The mean compressive strength of the masonry units in directions parallel and perpendicular to the perforations was derived from three compressive tests in each case. The bearing surfaces of the individual brick specimens were capped using a self-leveling, rapid-hardening cement mortar. For directions parallel and perpendicular to the perforations, the average values obtained were 8.9 MPa and 3.7 MPa, respectively.

Table 1 Summary of test results

Specimen notation	Peak load (kN)		Displacement at failure[a] (mm)		$\frac{P_{max}}{P_{max,C}}$	$\frac{\delta_u}{\delta_{u,C}}$	Cumulative dissipated energy (kN mm)		Failure mode (Failure direction)
	Push	Pull	Push	Pull					
Series A							Cycle 5	Cycle 10	
A_$C_{10\%}$	6.35	5.74	0.69	0.65	1.00	1.00	–	–	Rocking (Push)
A_$R1_{10\%}$	42.11	40.16	9.28	8.12	7.00	12.49	97.65	537.51	FRP fracture (Pull)
A_$R2_{10\%}$	44.31	43.21	7.52	7.77	6.98	10.90	86.12	669.79	Toe crushing (Push)
A_$M1_{10\%}$	32.23	30.52	9.29	9.39	5.08	13.46	94.81	474.36	Toe crushing (Push)
A_$M2_{10\%}$	39.18	36.25	9.36	9.00	6.17	13.57	103.64	583.00	Toe crushing (Push)
A_$NSM5_{10\%}$	6.47	6.35	0.85	0.66	1.02	1.23	–	–	Rocking (Push)
A_$C_{2.5\%}$	1.95	1.83	0.70	0.75	1.00	1.00	–	–	Rocking (Push)
A_$R1_{2.5\%}$	37.48	39.92	7.93	8.38	19.22	11.33	67.58	350.91	FRP fracture (Push)
A_$R2_{2.5\%}$	49.56	53.34	8.00	– [b]	25.42	11.43	91.71	435.22	Toe crushing (Push)
A_$M1_{2.5\%}$	25.27	24.29	11.44	10.37	13.27	13.83	83.44	365.39	Toe crushing (Pull)
A_$M2_{2.5\%}$	35.52	36.25	9.24	9.03	18.22	13.20	79.66	416.26	Toe crushing (Push)
Series B							Cycle 2	Cycle 3	
B_$C_{25\%}$	19.20	–	2.05	–	1.00	1.00	–	–	Flexure
B_$M1_{25\%}$	46.14	33.45	3.26	4.04[c]	2.40	1.59	31.98	92.45	Crushing[d] (Push)
B_$M2_{25\%}$	47.61	43.21	4.43	4.27	2.48	2.16	41.07	137.18	Crushing[d] (Push)
B_$C_{10\%}$	15.91	–	0.80	–	1.00	1.00	–	–	Flexure
B_$R1_{10\%}$	48.57	40.65	2.21	3.24	3.05	2.76	37.92	104.66	Crushing[d] (Push)
B_$M1_{10\%}$	41.74	31.10	5.18	6.79	2.62	6.48	34.46	88.67	Crushing[d] (Push)
B_$M2_{10\%}$	60.13	47.29	5.12	5.56	3.78	6.40	37.48	103.40	Crushing[d] (Push)
Series C							Cycle 2	Cycle 3	
C_C	8.24	–	0.82	–	1.00	1.00	–	–	Flexure
C_R1	58.62	49.69	2.08	3.45	7.11	2.54	43.34	118.17	Crushing[d] (Push)
C_M1	38.82	31.98	9.41	10.72	4.71	11.48	50.77	118.72	TRM debonding (Push)
C_M2	58.84	46.14	2.41	2.82	7.14	2.94	54.23	139.21	Crushing[d] (Push)

[a] Displacements are measured at top for Series A and at mid-span for Series B and C; for specimens which displayed rocking (A_$C_{10\%}$, A_$C_{2.5\%}$ and A_$NSM5_{10\%}$) δ_u corresponds to the point of heel lifting-off of the footing

[b] A threaded rod (part of the base fixing assembly) failed at pull direction

[c] Failure in the push direction did not permit completion of the displacement cycle; here, δ_u^- corresponds to 88% of P_{max}^-

[d] Brick crushing at mid-span

The cement:lime:sand proportions in the mortar used to bind the bricks were roughly 1:2:10, by volume, and the water to cement ratio was in the order of 0.8, by weight. The mortar strength was obtained through flexural and compression testing according to [17], using a servohydraulic MTS testing machine. Flexural testing was carried out on $40 \times 40 \times 160$ mm hardened mortar prisms, at an age of 28 days. The prisms were: (i) cast in steel moulds with three identical compartments, so that three specimens were available for each of the three days during which the walls were constructed; (ii) cured in the laboratory until testing, in conditions identical to those for the wall specimens; and (iii) subjected to three-point bending, at a span of 100 mm, with a constant loading rate equal to 5 N/s. The peak load was recorded and used for the calculation of flexural strength. Compression testing was carried out on each of the fractured parts of the prisms used in flexural testing, by means of two 40×40 mm bearing steel platens placed on top and bottom of each specimen part, which was carefully aligned so that the load was applied to the whole width of the faces in contact with the platens. The flexural and compressive strengths obtained from this procedure were 1.17 MPa and 3.91 MPa, respectively (mean values of all prisms tested).

For the specimens receiving externally bonded strengthening, a commercial textile with equal quantity of high-strength carbon fiber rovings in two orthogonal directions was used (Fig. 2a). The

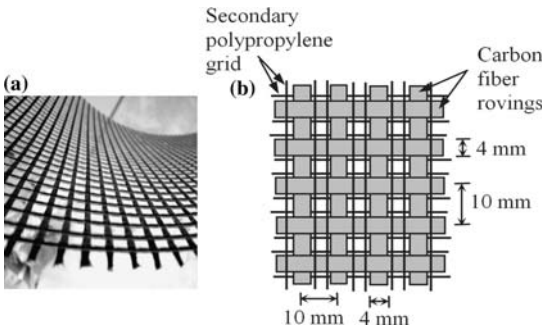

Fig. 2 (**a**) Photograph; and (**b**) architecture of bi-directional textile used in this study

fiber rovings were not interwoven, but were simply placed one on top of the other and connected through a secondary polypropylene grid (see Fig. 2b for the arrangement of the carbon rovings). Each roving was 4 mm wide and the clear spacing between rovings was 6 mm. The weight of carbon fibers in the textile was 168 g/m^2 and the nominal thickness of each layer (assuming equivalent smeared distribution of the fibers) was 0.047 mm. The guaranteed tensile strength of the carbon fibers (as well as of the textile, when the nominal thickness is used) in each direction was taken from the data sheets supplied by the producer equal to 3,350 MPa. The elastic modulus of carbon fibers was 225 GPa.

For the specimens receiving mortar as binding material, a commercial inorganic dry binder was used, consisting of cement and polymers at a ratio of 10:1 by weight; the binder to water ratio was 3.3:1 by weight. The resulting consistency was plastic providing good workability, such that application on vertical surfaces using a trowel was easily achieved. The workability retention period was approximately half an hour in ambient temperature (20°C). The binder's flexural and compressive strengths (5.77 MPa and 31.36 MPa, respectively) were obtained following a procedure identical to the one described for the general purpose masonry mortar, using triplets of mortar prisms taken on each day textile application took place. For the specimens receiving adhesive bonding, a commercial structural adhesive (two-part epoxy resin with a mixing ratio 4:1 by weight) was used. According to the product sheet, the tensile strength and the elastic modulus of the adhesive (cured for 7 days at 23°C) were 30 MPa and 3.8 GPa, respectively. The adhesive was pasty and viscous enough so that complete wetting of the fibers in the textile was possible by using a plastic roller.

For the specimen of Series A receiving NSM reinforcement, grooves were formed along the bed joints designated to receive the CFRP strips by scraping-off part of the bed mortar, while the latter was still in a fresh state. Prior to the application of the NSM strips, the grooves were thoroughly cleaned using compressed air and dampened through water spraying. Then, they were filled with a fixing cement-based mortar taking care to avoid air entrapment, and the strips, which extended the full length of the specimen, were inserted in the grooves (seated on face) until full embedment was achieved. Finally, any excess fixing mortar was removed and the grooves' face was made even with the face of the wall using a trowel. The fixing mortar comprised a three-part material consisting of epoxy resin suspensions, cement and supplementary cementitious materials. Its consistency allowed for vertical application, whereas its compressive and flexural strengths (as provided by the producer data sheets) were 40 MPa and 9 MPa, respectively.

Commercially available tape-like CFRP strips specifically designed for NSM strengthening were used. The strips with a cross section of 2 × 16 mm were furnished in 76 m long spools and consisted of carbon fibers in a bisphenol epoxy vinyl ester resin matrix. The elastic modulus and volumetric ratio of carbon fibers in the CFRP strips were equal to 225 GPa and 40%, respectively. The guaranteed tensile strength, the elastic modulus and the ultimate strain of the CFRP strips were taken from data sheets of the producer equal to 2,070 MPa, 125 GPa and 0.17%, respectively. For the sake of scaling down, each NSM strip was cut in two pieces (along the length) using a thin saw; the resulting strips had a width of 7.5 mm.

In order to avoid premature failure due to handling and positioning of the unjacketed specimens (that is the control and the one with NSM strips), a 15 mm thick plaster layer was applied on their faces following a double-coat procedure: the undercoat was forcefully thrown on the damp

masonry surface (using a hand-held trowel), in order to improve adhesion, and the second coat was applied while the first one was still fresh but relatively firm. The commercial dry cement-based mix used for plastering had a 28-days compressive strength of approximately 4 MPa.

The application of the textile layers was carried out ''as usual'', that is following a procedure similar to the one applicable for conventional FRP interventions. Each specimen was first ground at points where mortar was protruding from the brickwork face and brushed clean; then, dust and any loose particles were removed with high air pressure and, finally, the textile sheets were bonded on both sides of the wall (covering the entire surface of each side) by implementation of a standard wet lay-up procedure. The procedure included the following steps: (i) application of the bonding agent (either epoxy or mortar) on the wall surface (which was dampened for specimens receiving mortar); (ii) bonding of the textile by hand and roller pressure; and (iii) application of the bonding agent in between layers (in case of two layers), while the previous layer was still in a fresh state, as well as on top of the last textile sheet. Mortar was applied in approximately 2 mm thick layers, using a smooth metal trowel, and the textile was slightly pressed into the mortar, so that mortar protrusion through all the perforations between fiber rovings was ensured. Curing of the bonding agents was achieved in room conditions. A typical photograph of the application method of textile sheets combined with mortar binder on wall specimens is shown in Fig. 3.

In order to measure the compressive strength of the walls in directions parallel and perpendicular to the bed joints, six small wall assemblages were constructed and tested under monotonic uniaxial compression (three specimens were used for each loading direction). These two bricks long by six bricks high masonry prisms, measuring $390 \times 85 \times 420$ mm (length $\times$ width $\times$ height), were constructed using the same bricks, mortar and bond type (that is running bond) as for the rest of the specimens used in the experimental program. It should be noted that all types of wall specimens (including wall prisms) were constructed and tested during the same time spans.

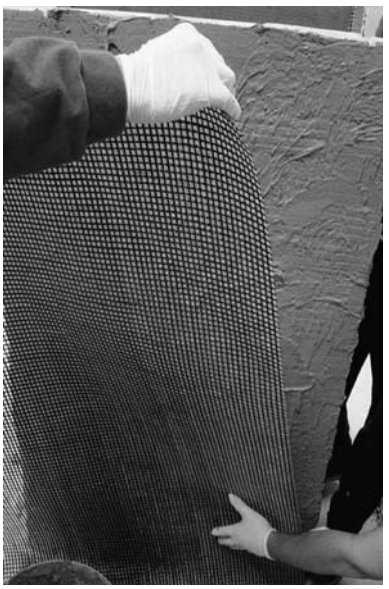

Fig. 3 Application of the textile reinforcement onto the cementitious mortar

The surfaces of the prisms which were in contact with the testing machine's platens were capped using a normal strength cement mortar, in order to ensure a uniform load transfer. The compression tests were carried out in displacement control mode at a constant loading rate equal to 0.1 mm/s, using a 4,000 kN loading capacity testing machine. Loads were measured from a load cell and displacements were obtained using external linear variable differential transducers (LVDTs) with a stroke of 5 mm. The LVDTs were mounted at mid-height, at a gauge length of approximately 130 mm. The mean values of the compressive strength, secant modulus of elasticity (at maximum stress) and ultimate strain derived from compressive loading parallel to the bed joints were 4.3 MPa, 1.94 GPa and 0.22% respectively. The corresponding values for compressive loading perpendicular to the bed joints were 2.0 MPa, 1.70 GPa and 0.12%, respectively.

As expected, due to the different strength characteristics of the masonry walls in two orthogonal directions (perpendicular and parallel to the bed joints), the uniaxial strength of the walls in these directions was found to be different. More specifically, failure due to loading parallel to the bed joints was brittle as a result of crushing

of the outer brick cells. For compression perpendicular to the bed joints, failure was less sudden than for the previous case and was manifested through vertical cracks running along the height of the walls, crossing the bed joints.

2.3 Test set-up, instrumentation and procedure

All specimens were subjected to cyclic in-plane loading using a stiff steel frame, except for the control ones in Series B and C ($B\_C_{10\%}$, $B\_C_{25\%}$ and C_C), which were tested monotonically. Series A specimens were tested as vertical cantilevers with a concentrated force at the top, at a distance of 1.10 m from the fixed base; Series B and C specimens were tested as horizontal beams in three-point bending, at a span of 1.17 m and 1.12 m, respectively.

The test set-up for Series A specimens (shear walls) is shown in Fig. 4. Fixing of the walls on the steel frame along their base was ensured through encasing their lower rows in a 'footing' comprising a set of four steel tubes which were firmly attached on the frame's base plate. The voids between the footing and the wall were filled with epoxy resin (along the wall's faces) and a non-shrinking, high strength, rapid-hardening mortar (at the wall's ends). In order to ensure uniform load transfer at the top of the walls a steel capping system was devised; the connection between the wall and the capping was achieved by the same means as for the connection between the wall and the footing. The load was applied using a horizontally positioned 250 kN MTS actuator which was connected to the capping system through a pair of threaded rods (22 mm in diameter). The vertical force exerted on the specimens at the position where the actuator was mounted on the capping system, due to the actuator's self-weight, was balanced by a series of weights which were stacked and fixed in position at the opposite (to the actuator's) side. The application of compressive stress corresponding to 10% of compressive strength was achieved using a system of two single-acting, low-height hydraulic cylinders (with a capacity of 120 kN). Each cylinder was clamped through the use of a pair of threaded rods between the capping and the testing frame's base plate. The hydraulic system allowed for the regulation and automated adjustment of the applied pressure to the specified level and its continuous monitoring through a digital pressure gauge. The compressive stress at 2.5% of the masonry strength was exerted by simply stacking and fixing weights on top of the capping. Five external rectilinear displacement transducers were used to measure the walls' horizontal displacements at distance of 0.20, 0.55 and 0.85 m from the fixed support, as well as to monitor the probable uplift at the base, as shown in Fig. 4.

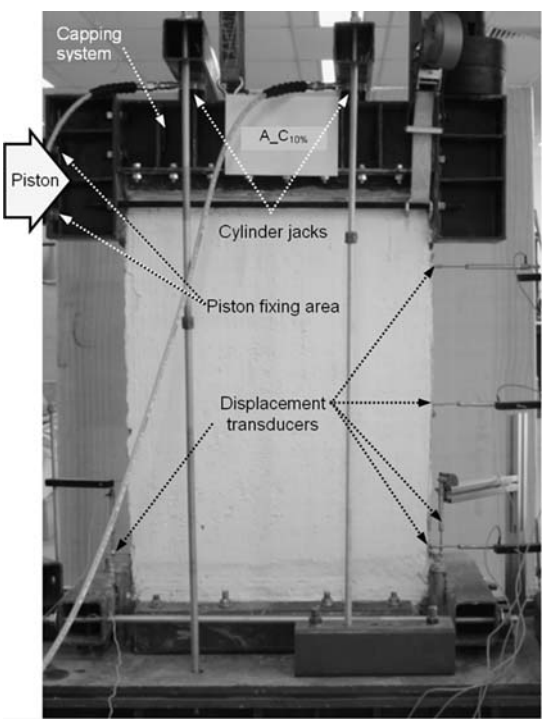

Fig. 4 Experimental setup for Series A specimens

Wall specimens of Series B were subjected to in-plane three-point bending at a total span of 1.17 m, while an axial load was applied on their outer brick rows and kept constant throughout the duration of the test. The test arrangement aimed at reproducing the in-plane flexure/shear seismic loading of pilasters found in the lower levels of masonry structures, where axial loads may be considerable. Two pairs of steel hinges were placed at each support (along the specimens' thickness, at top and bottom) and a third

one was placed at mid-span (that is along the load application line). At least one week prior to testing, six 100 mm wide and 20 mm thick bands of high strength mortar had been cast on the specimens' bearing areas (three per side), in order to compensate for any surface unevenness and to ensure uniformity of load transfer. Attention was given so that immediate contact of the externally bonded layers of textile reinforcement and the load-bearing areas was avoided. For the application of the axial load, a hydraulic cylinder identical to the ones used for Series A specimens was used, in combination with a custom-made confining system comprising a pair of horizontally placed threaded rods. The test set-up for Series B specimens is shown in Fig. 5. The displacement-control loading protocol was applied using a vertically positioned 500 kN MTS actuator and displacements were measured at mid-span using an external rectilinear displacement transducer (of 25 mm stroke capacity) mounted at mid-height of the specimens. Data from the load cell and the displacement transducers (the piston's and the external one) were recorded using a fully computerized data acquisition system. The resulting load—mid-span displacement and load—piston displacement loops were generated by the system in real time.

The test set-up for specimens in Series C was practically identical with that in Series B, except that no axial loading was applied and the span was slightly different (1.12 m). For these specimens, the test arrangement intended to simulate in-plane flexure/shear loading typically applied in lintels during seismic excitations.

All specimens, except for the control ones of Series B (B_$C_{10\%}$, B_$C_{25\%}$) and Series C (C_C), were tested by applying the load in a quasistatic cyclic pattern of controlled displacements at a rate of 0.1 mm/s for specimens of Series A and 0.01 mm/sec for specimens of Series B and C. Specimens B_$C_{10\%}$, B_$C_{25\%}$ and C_C were tested under monotonically applied loading, in a displacement control mode at a rate of 0.003 mm/s. The cyclic loading sequence consisted of cycles at a series of progressively increasing displacement amplitudes in both directions (push and pull). The displacement amplitude increment was 1 mm and a single loading cycle was applied for each amplitude level, as illustrated in Fig. 6. The test was run in a fully computerized manner and was completed (manually terminated by returning the piston to zero position) when the ultimate capacity of the wall was reached and a considerable load reduction was evidenced in either direction (push or pull).

3 Results and discussion

The results are discussed based on the load versus in-plane displacement response. Peak load values in the push and pull directions, P^{+}_{max} and P^{-}_{max}, displacements at failure, δ^{+}_{u} and δ^{-}_{u}, (defined as the point of the load versus displacement envelope curve where either sudden load reduction was

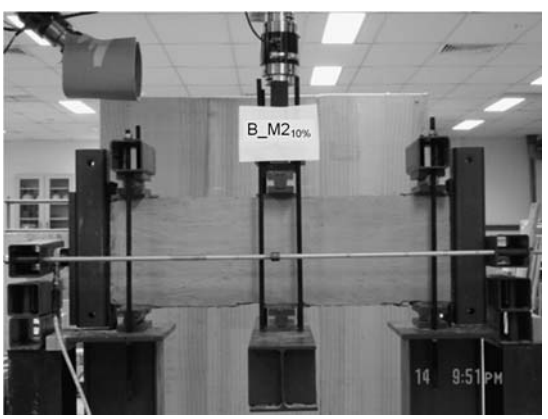

Fig. 5 Experimental set-up for Series B and C specimens (the system for axial load is not applicable for Series C specimens)

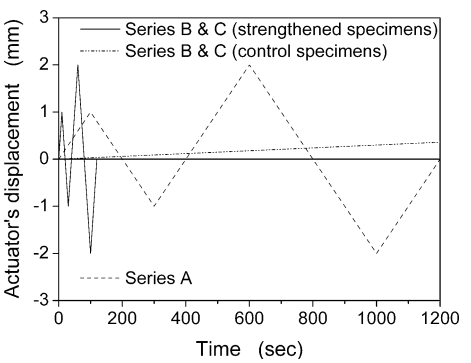

Fig. 6 Displacement histories (only the first two cycles are shown)

detected, or a 20% reduction in load was noted in specimens with gradual post-peak load reduction), cumulative energy dissipation capacity, observed failure modes and loading directions when failure occurred are given in Table 1, for all specimens. The displacements recorded in Table 1 are those at piston position for specimens of Series A (as extrapolated by the displacement profile obtained from the three horizontal displacement transducers), and at mid-span for specimens of Series B and C. In the load versus displacement plots (hysteresis loops and envelope curves), displacement values in the push direction, that is outward movement of the piston, are taken positive.

Table 1 also gives the ratios of $P_{max}/P_{max,C}$ and $\delta_u/\delta_{u,C}$, where P_{max} is the peak load in the direction where failure was detected first and δ_u is the displacement at ultimate (in the respective direction); $P_{max,C}$ and $\delta_{u,C}$ are the same values for the control specimens.

3.1 Series A—shear walls

The load versus top displacement hysteresis loops for Series A specimens are given in Fig. 7a–i. The

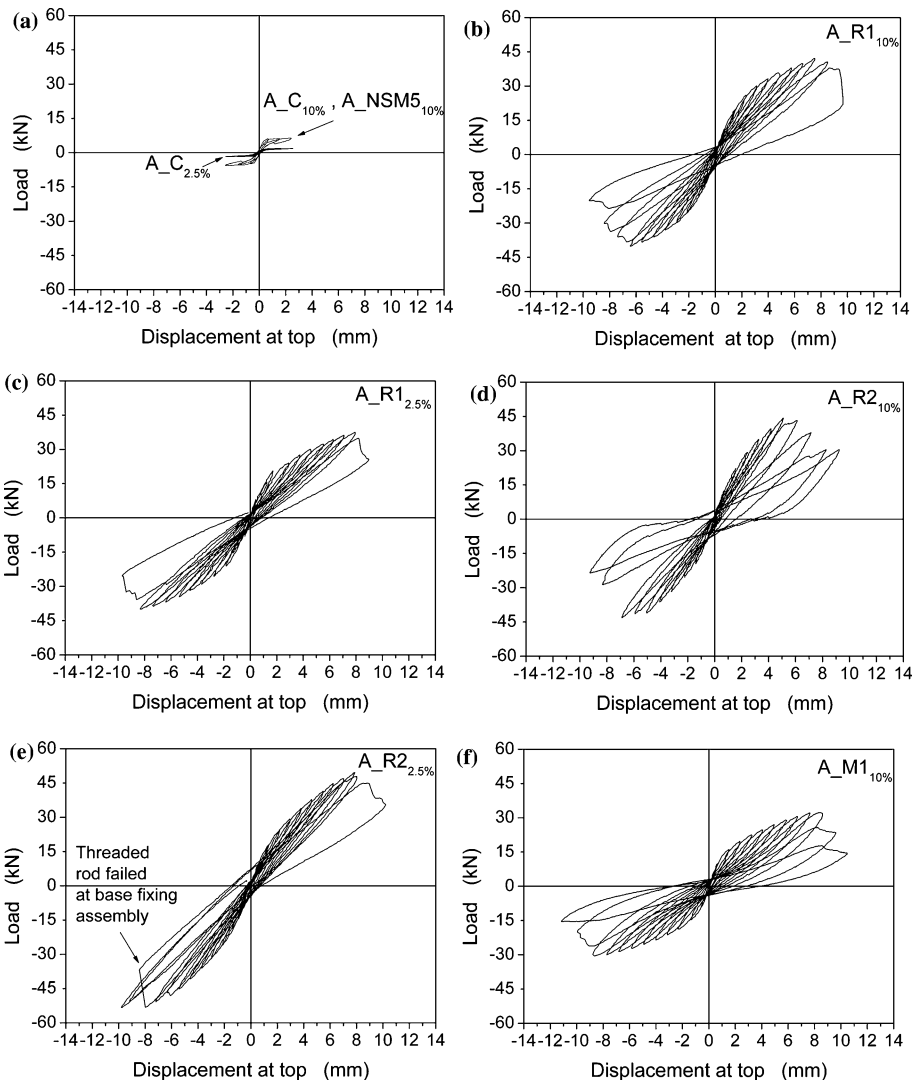

Fig. 7 Series A results: (**a**)–(**i**) Load versus top displacement hysteresis loops; (**j**)–(**k**) envelope curves

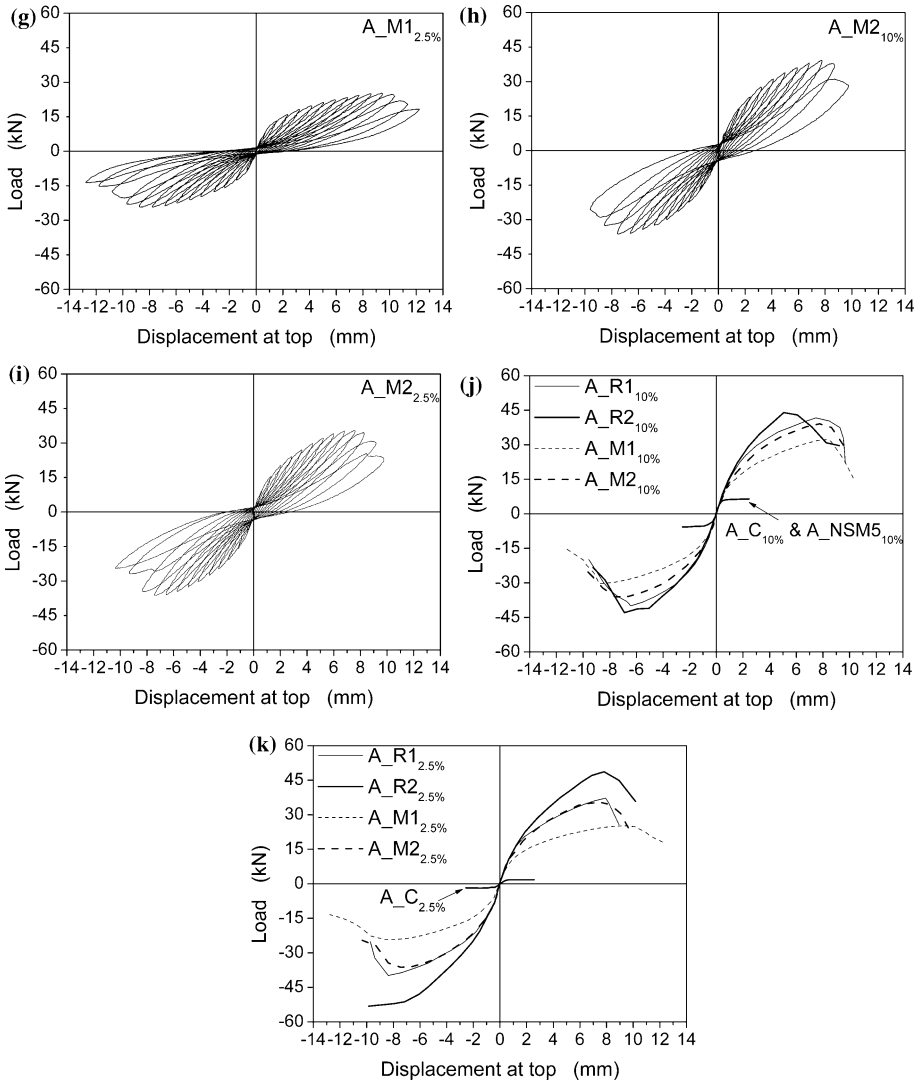

Fig. 7 continued

control specimen of Series A bearing a compressive stress equal to 0.2 MPa (that is specimen A_$C_{10\%}$) displayed rocking characteristics as a follow-up of extensive horizontal cracking near the base. A nearly rigid body rotation of the wall was observed, centering on the specimen's toes (just above the fixing assemblage), where large horizontal cracks were formed and run along two consecutive bed joints. In Fig. 7a, the change in the slope indicates the points at which the heel lifted off of the footing (these points also account for δ_u^+ and δ_u^-, in the push and the pull direction, respectively). Peak recorded loads were equal to 6.35 kN and 5.74 kN in the push and the pull direction, respectively, whereas the corresponding displacements (measured at top) were equal to 0.69 mm (push) and 0.65 (pull).

The response of specimen A_$C_{2.5\%}$ was identical to the one described above, with the peak recorded loads being equal to 1.95 kN (push) and 1.83 kN (pull), that is approximately 70% less than those for specimen A_$C_{10\%}$; the displacements at top corresponding to the wall's uplift were measured equal to 0.70 mm (push) and 0.75 mm (pull). This type of failure mode in specimens A_$C_{10\%}$ and A_$C_{2.5\%}$ is attributed to

the relatively low levels of the axial load applied and the moderate slenderness of the specimens (the walls' aspect ratio, that is the height over width ratio, was equal to 1.4).

Since rocking was proved to be the predominant mode of failure of the unreinforced masonry shear walls, it was not surprising that horizontally placed NSM reinforcements failed to provide any load bearing capacity increase. Indeed, specimen A_NSM5$_{10\%}$ failed at a maximum lateral load of 6.47 kN in the push direction (practically equal to the corresponding value for A_C$_{10\%}$ specimen), due to rocking. As shown in Fig. 7a, the load—top displacement loops for specimen A_NSM5$_{10\%}$ coincide with the ones for specimen A_C$_{10\%}$. The NSM reinforcement would have been able to enhance the wall's load-bearing capacity if the predominant failure mode of the unreinforced specimens was diagonal tension; in this case, the horizontally placed strips would have performed as crack arrestors.

The responses of the two specimens symmetrically strengthened with one layer of resin-bonded textile (A_R1$_{10\%}$ and A_R1$_{2.5\%}$) were found to be identical in terms of damage progression and failure mode. More specifically, during the initial stage of loading (first couple of cycles) flexural cracking at brick—bed joint interfaces was detected. During subsequent displacement cycles and until the peak load was reached, progressive vertical cracking of the brick webs at the walls' toes was evidenced, which was attributed to compression. Following extensive toe damage (fairly symmetrical in both the push and pull directions), tensile fracture of the textile took place (at the furthermost tensioned side of the specimen) just above the walls' base (Fig. 8a); this led to complete crushing of the toe brickwork under compression and to the local buckling of the textile at this point (Fig. 8b), which in turn resulted in substantial load reduction (Fig. 7b, c). Specimen A_R1$_{10\%}$ failed in the pull direction at a peak load of 40.16 kN and a top displacement of 8.12 mm, whereas specimen A_R1$_{2.5\%}$ failed in the push direction at a peak load of 37.48 kN and a top displacement of 7.93 mm. Comparison of the aforementioned values reveals that the higher axial load, in walls with single-layer resin-based jackets, gave a marginally higher strength (by 7%) and an insignificant increase in deformability (by 2%).

Specimens A_R2$_{10\%}$ and A_R2$_{2.5\%}$ (Fig. 7d, e) responded in a similar way to their single-layer counterparts, the only differences being in their stiffer behavior (after flexural cracking at the bed joints) and the absence of fiber rupture prior to toe crushing/jacket buckling. Furthermore, due to the higher uplift recorded for specimen A_R2$_{10\%}$ (in regards to the rest of the specimens receiving resin-impregnated jackets), failure for this wall was rather premature, at relatively low load and displacement values. Peak loads at failure for specimens A_R2$_{10\%}$ and A_R2$_{2.5\%}$ (both in the push direction) were recorded equal to 44.31 kN and 49.56 kN, respectively; top displacements at failure were equal to 7.52 mm (A_R2$_{10\%}$) and 8.00 mm (A_R2$_{2.5\%}$). Here the higher axial load gave marginally decreased values of strength and ultimate displacement. Compared to single-layer jackets, the double-layer ones resulted in higher strength (the difference was about 30% at low axial load and about 10% at the higher one) and slightly reduced deformability.

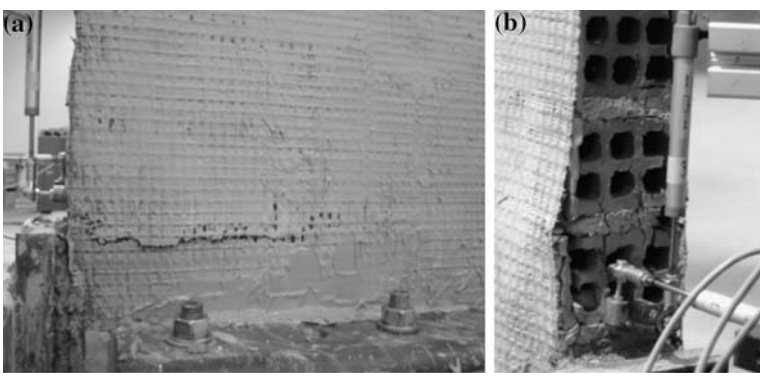

Fig. 8 Failure mode of specimen A_R1$_{2.5\%}$: (**a**) Jacket rupture in tension; and (**b**) toe crushing/ jacket buckling in compression

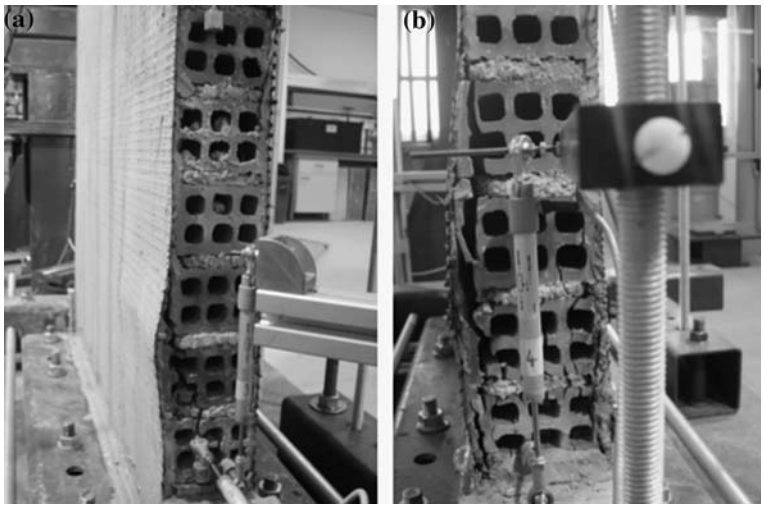

Fig. 9 Failure mode of specimen A_M2$_{10\%}$: Toe crushing and jacket buckling in (**a**) push and (**b**) pull direction

The walls strengthened with TRM jackets showed no distinct differences compared to those strengthened with resin-impregnated ones in terms of damage development and failure mode. During testing of specimens A_M1$_{10\%}$ and A_M1$_{2.5\%}$ (Fig. 7f, g), gradual rupture of discrete fiber bundles took place just above the walls' base, accompanied by matrix cracking. Textile rupture was more extensive for specimen A_M1$_{2.5\%}$ than for specimen A_M1$_{10\%}$. During testing of specimen A_M1$_{2.5\%}$ and after the first couple of load reversals, a pattern of evenly spaced horizontal fine cracks on the wall's face was visible near the base. The recorded peak loads at failure for specimens A_M1$_{10\%}$ (push direction) and A_M1$_{2.5\%}$ (pull direction) were 32.23 kN and 24.29 kN, respectively; top displacements at ultimate were equal to 9.29 mm (A_M1$_{10\%}$) and 10.37 mm (A_M1$_{2.5\%}$). These values show that the higher axial load resulted in an increase of the load-bearing capacity (in the order of 33%) and entailed a small deformability penalty, in the order of 10%. Compared to their resin-impregnated counterparts, mortar-impregnated single-layer jackets resulted in lower effectiveness in terms of strength but in higher in terms of deformability. More precisely, the strength was reduced in specimen A_M1$_{10\%}$ (compared to specimen A_R1$_{10\%}$) by 20% and in specimen A_M1$_{2.5\%}$ (compared to specimen A_R1$_{2.5\%}$) by 35%; the corresponding increases in deformability amounted to 14% and 31%, respectively.

Specimens with double-layer TRM jackets responded similarly to their resin counterparts. The failure mode (toe crushing) of specimen A_M2$_{10\%}$ is shown in Fig. 9. The load versus top displacement plots (hysteresis loops are given in Fig. 7h, i and envelope curves in Fig. 7j, k) depict the notably reduced stiffness of TRM jackets in comparison to resin-impregnated ones, due to microcracking of the cement-based matrix. The recorded peak loads at failure for specimens A_M2$_{10\%}$ and A_M2$_{2.5\%}$ (both in the push direction) were 39.18 kN and 35.52 kN, respectively; top displacements at ultimate were equal to 9.36 mm (A_M2$_{10\%}$) and 9.24 mm (A_M2$_{2.5\%}$). These values show that the higher axial load resulted in a marginal increase of the load-bearing capacity (in the order of 10%), whereas the deformability remained practically unaffected. Compared to single-layer (mortar-based) jackets, the double-layer ones resulted in higher strength (the difference was about 45% at low axial load and 22% at the higher one) and in slightly reduced deformability.

Compared to their resin-impregnated counterparts, mortar-impregnated double-layer jackets resulted in lower effectiveness in terms of strength but in higher in terms of deformability. More precisely, the strength was reduced in specimen A_M2$_{10\%}$ (compared to specimen A_R2$_{10\%}$) by 12% and in specimen A_M2$_{2.5\%}$ (compared to specimen A_R2$_{2.5\%}$) by 28%; the

corresponding increases in deformability amounted to 24% and 16%, respectively.

By comparison of the cumulative dissipated energies given in Table 1 for the fifth and the tenth displacement cycles (computed by summing up the area enclosed within the load versus piston displacement curves), it is concluded that the energy dissipation capacity of the TRM-based strengthening scheme is comparable to the one of the FRP-based.

Overall, it is concluded that TRM jacketing was extremely effective. On a strength basis the effectiveness of TRM versus FRP is lower, between 12% and 30%, depending on the number of layers and the level of axial load; but on a deformability basis, of high importance in seismic design, it is higher, between 14% and 31%, depending on the number of layers and the level of axial load.

3.2 Series B—beam-columns

The load versus mid-span displacement hysteresis loops and the envelope curves for specimens in Series B are given in Fig. 10a–d. Both control specimens ($B\_C_{25\%}$ and $B\_C_{10\%}$) of this series failed due to the development of a single flexural crack which was formed along the bed joint closest to the mid-span. The crack run along the brick/mortar interface, indicating that bond strength in the joints was governed by brick/mortar adhesion rather than by the tensile strength of the mortar. Specimen $B\_C_{25\%}$ failed at a peak load of 19.2 kN, which was approximately 20% higher than the peak load (15.91 kN) recorded for specimen $B\_C_{10\%}$. Mid-span displacements at failure were equal to 2.05 mm and 0.80 mm for specimens $B\_C_{25\%}$ and $B\_C_{10\%}$, respectively.

The response of specimens strengthened with a single layer of TRM jacketing ($B\_M1_{25\%}$ and $B\_M1_{10\%}$) during the first couple of displacement cycles was characterized by flexural cracking (brick/mortar debonding at bed joints near the mid-span), as shown in Fig. 11a. In subsequent piston reversals, gradual cracking of the brick webs in the compression zones near the mid-span was detected. The cracks, which run parallel to

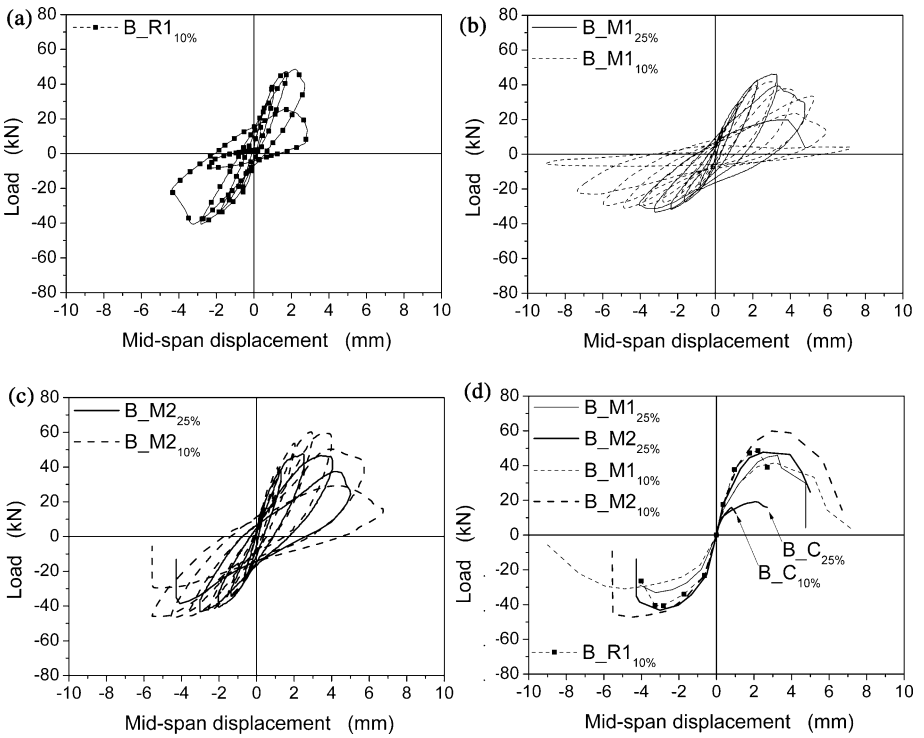

Fig. 10 Series B results: (**a**)–(**c**) Load versus mid-span displacement hysteresis loops; (**d**) envelope curves

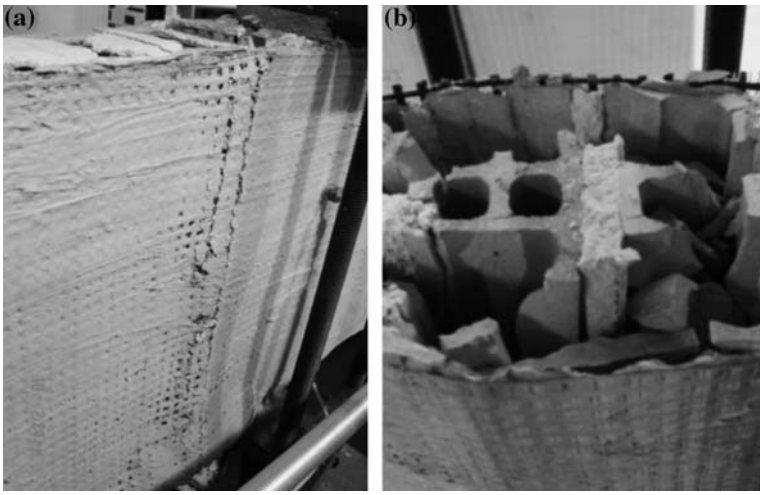

Fig. 11 (**a**) Flexural cracking in specimen B_M1$_{10\%}$, prior to brick crushing; (**b**) brick crushing in specimen B_R1$_{10\%}$ (photo taken after removal of the load application fixture)

the specimens' longitudinal axis, crossed the bed joints and resulted in complete compressive crushing; this was simultaneously followed by outward buckling of the unsupported jacket. Failure for specimen B_M1$_{25\%}$ occurred in the push direction at a peak load equal to 46.14 kN and a displacement equal to 3.26 mm. The corresponding values for specimen B_M1$_{10\%}$ (also recorded in the push direction) were 41.74 kN and 5.18 mm. By comparison of the aforementioned values it can be stated that an increase of the axial load resulted in a small increase of strength (by 11%) and in a considerable decrease of deformability (by 37%).

The response of specimen B_R1$_{10\%}$ (which had received a single layer of FRP jacketing) differed from that of its mortar-based counterpart only in the fact that during the initial stages of loading flexural cracking (brick/mortar debonding) was not visible. Otherwise, the damage sequence was similar to that of specimen B_M1$_{10\%}$ (Fig. 11b illustrates the specimen's failure). The peak load at failure was 48.57 kN (in the push direction) and the corresponding displacement was 2.21 mm. By comparison to specimen B_R1$_{10\%}$, the TRM-strengthened wall, displayed a rather small decrease in strength (equal to 14%) and a very large increase in deformability, equal to 134%.

For the walls receiving double-layer mortar-impregnated jackets, failure was attributed to the same mechanisms as described above (flexural cracking at bed joints followed by brick compressive crushing at mid-span). Specimen B_M2$_{25\%}$ failed under a peak load of 47.61 kN (in the push direction) and a corresponding displacement of 4.43 mm, whereas the respective values recorded for specimen B_M2$_{10\%}$ (also in the push direction) were 60.13 kN and 5.12 mm. Additionally, for the lower axial load, double-layer jackets—compared to single-layer ones—resulted in a substantial increase of strength (by 44%), the deformability being kept almost identical. However, for the higher axial load, double-layer jackets gave a marginal increase in strength (by 3%) but higher deformability (by 36%).

By comparison of the cumulative dissipated energies given in Table 1 for the second and the third displacement cycles, it is concluded that, in general, the energy dissipation capacity of the two strengthening schemes (FRP versus TRM, specimens B_R1$_{10\%}$ versus B_M1$_{10\%}$) is similar.

3.3 Series C—beams

The load versus mid-span displacement hysteresis loops and the envelope curves for specimens in Series C are given in Fig. 12a–d. The control specimen of this series failed at a peak load of 8.24 kN under a single flexural crack, formed at the brick-head joint interfaces closest to the mid-span. Visual inspection revealed that the crack propagated stepwise through some of the bed joints (in the longitudinal direction), without

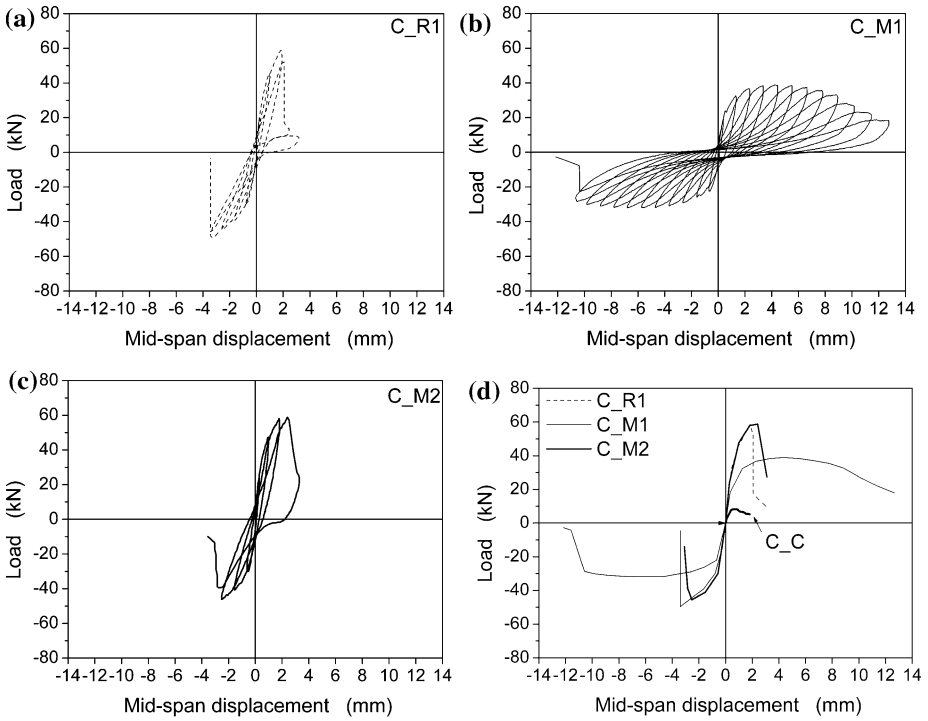

Fig. 12 Series C results: (**a**)–(**c**) Load versus mid-span displacement hysteresis loops; (**d**) envelope curves

causing fracture of the bricks. The mid-span displacement at failure was equal to 0.82 mm.

During the first loading cycle of specimen C_R1, flexural cracks were formed in the vicinity of the mid-span denoting brick-head joint debonding, the full development of which was prevented by the jacket. In the subsequent cycles, limited debonding at the interface between the external shells of the central bricks and the jacket was taking place in the compression side of each cycle (Fig. 13a), resulting in sudden crushing of the bricks at mid-span, also manifested by a sudden load reduction (Fig. 12a). Peak load and mid-span displacement at failure (resulting in the push direction) were equal to 58.62 kN and 2.08 mm, respectively.

The response of specimen C_M1 (Fig. 12b) was found to be different from the one of its resin-impregnated counterpart in the sense that flexural cracking was more distributed (and visible due to cracking of the mortar) and debonding at the interface between the external shells of the bricks and the jacket (Fig. 13b) was more extensive. Failure occurred during the ninth displacement cycle in the push direction, when the bricks in the compression zone at mid-span crushed. At this point, the debonded textile area was extending almost to the edge supports and reached more than 60 mm along the specimen's height in both the push and pull directions. Additionally, a small fraction of the fiber rovings had ruptured, providing evidence of the textile's full mobilization. Owing to flexural crack spreading, as well as to both gradual debonding and discrete fiber fracture, the load versus mid-span displacement envelope curve (Fig. 12d) of specimen C_M1 displayed substantial ductility characteristics. The maximum recorded load in the push direction was equal to 38.82 kN and the mid-span displacement at ultimate was 9.41 mm. In comparison with specimen C_R1 (resin-based jacket) these values correspond to a 34% reduction in strength but a 350% increase in deformability.

Specimen C_M2 responded in a way similar to specimen C_R1, failing due to compressive crushing of the bricks at mid-span. The peak load at failure was equal to 58.84 kN and the corresponding mid-span displacement was 2.41 mm.

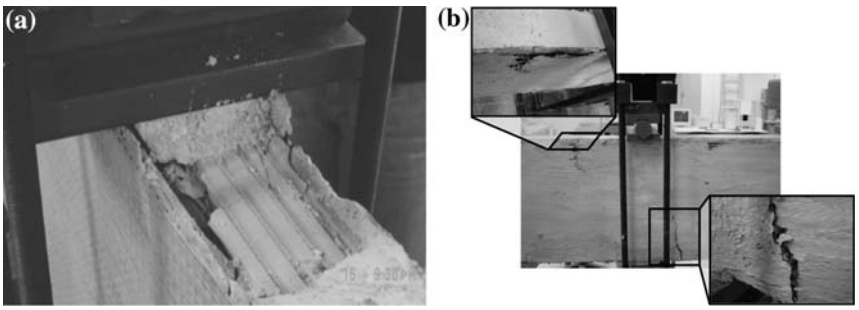

Fig. 13 (**a**) Limited debonding of the jacket and brick compressive crushing near the mid-span (specimen C_R1); (**b**) Flexural cracking (of the wall and the jacket's mortar) and extensive debonding of the TRM jacket from specimen's C_M1 surface

By comparing the results with those for specimen C_M1, it is concluded that the use of two textile layers per side, instead of a single one, led to a strength increase by 52%, which, as expected, entailed a penalty in deformability, here in the order of 74%.

Finally, comparison of the cumulative dissipated energies given in Table 1 for the second and the third displacement cycles leads to the conclusion that, in general, the energy dissipation capacity of walls with TRM jacketing is at least as high as that of walls with FRP jacketing.

4 Conclusions

Based on the response of medium-scale clay brick shear walls, beam-column type walls and beam type walls subjected to cyclic in-plane loading, it is concluded that TRM overlays provide a substantial gain in strength and deformability. Compared with resin-based systems, TRMs result in reduced effectiveness for strength, the magnitude of which depends on the type of loading and on the number of textile layers used. From the experimental results obtained herein it may be stated that, in terms of strength, TRM jackets are at least 65–70% as effective as FRP jackets with identical fiber configurations. In terms of deformability, of crucial importance in seismic retrofitting of unreinforced masonry walls, TRM jacketing is much more effective than FRP. The increased effectiveness is about 15–30% in shear walls, 135% in beam-column type walls and 350% in beam type walls, on the basis of tests conducted in this study. Moreover, regardless of the matrix material (mortar versus resin), the strength generally increases with the number of layers and the axial load, at the expense of deformability.

From the results obtained in this investigation the authors believe that TRM jacketing is an extremely promising solution for strengthening and seismic retrofitting of unreinforced masonry walls subjected to in-plane loading. Further study is needed in order to enhance the experimental database and to optimize the TRM-based strengthening system.

Acknowledgements The authors wish to thank Mrs. M. Bouzoukou and Mr. C. Bavellas for their assistance in the experimental program. The work reported in this paper was partially funded by the Greek General Secretariat for Research and Technology, through the project ARISTION, within the framework of the program ''Built Environment and Management of Seismic Risk''.

References

1. Papanicolaou CG, Triantafillou TC, Karlos K, Papathanasiou M (2006) Textile reinforced mortar (TRM) versus FRP as strengthening material of URM walls: out-of-plane cyclic loading. Mater Struct (submitted)
2. ACI 549.2R-04 (2004) Report on thin reinforced cementitious products. Reported by ACI Committee 549, American Concrete Institute, Farmington Hills, Michigan
3. Bischoff T, Wulfhorst B, Franzke G, Offermann P, Bartl A-M, Fuchs H, Hempel R, Curbach M, Pachow U, Weiser W (1998) Textile reinforced concrete façade elements – An investigation to optimize concrete

composite technologies. In: Proceedings of the 43rd International SAMPE Symposium. pp 1790–1802
4. Curbach M, Jesse F (1999) High-performance textile-reinforced concrete. Struct Eng Int IABSE 4:289–291
5. Brameshuber W, Brockmann J, Roessler G (2001) Textile reinforced concrete for formwork elements – Investigations of structural behaviour. In: Burgoyne CJ (ed) FRPRCS5. 5th International conference on fibre-reinforced plastics for reinforced concrete structures. Thomas Telford, Cambridge, UK, July 2001, pp 1019–1026
6. Naaman AE (2003) Progress in ferrocement and textile hybrid composites. In: Curbach M (ed) Proceedings of the 2nd colloquium on textile reinforced structures. Dresden, Germany, September 2003, pp 325–346
7. Reinhardt HW, Krueger M, Grosse CU (2003) Concrete prestressed with textile fabric. J Adv Concrete Technol 1(3):231–239
8. Curbach M, Ortlepp R (2003) Besonderheiten des verbundverhaltens von verstaerkungsschichten aus textilbewehrtem. In: Curbach M (ed) Proceedings of the 2 nd colloquium on textile reinforced structures. Dresden, Germany, September 2003, pp 361–374 (in German)
9. Curbach M, Brueckner A (2003) Textile strukturen zur querkraftverstaerkung von stahlbetonbauteilen. In: Curbach M (ed) Proceedings of the 2nd colloquium on textile reinforced structures. Dresden, Germany, September 2003, pp 347–360 (in German)
10. Brueckner A, Ortlepp R, Weiland S, Curbach M (2005) Shear strengthening with textile reinforced concrete. In: Hamelin P (ed) CCC 2005: 3rd international conference on composites in construction. July 2005, Lyon, France, pp 1307–1314
11. Triantafillou TC, Papanicolaou CG (2005) Textile reinforced mortars (TRM) as strengthening materials for concrete structures. In: Balazs GL, Borosnyoi A (eds) Proceedings of the fib symposium ''Keep Concrete Attractive''. Budapest, Hungary, May 2005, pp 345–350
12. Triantafillou TC, Papanicolaou CG (2006) Shear strengthening of reinforced concrete members with textile reinforced mortar (TRM) jackets. Mater Struct 39(1):85–93
13. Triantafillou TC, Papanicolaou CG, Zissimopoulos P, Laourdekis T (2006) Concrete confinement with textile reinforced mortar (TRM) jackets. ACI Struct J 103(1):28–37
14. Faella C, Martinelli E, Nigro E, Paciello S (2004) Tuff masonry walls strengthened with a new kind of C-FRP sheet: experimental tests and analysis. In: Proceedings of the 13th world conference on earthquake engineering. paper no. 923
15. Krevaikas T (2005) Strengthening of unreinforced masonry structures with advanced composites. PhD Dissertation, Dept of Civil Engineering, University of Patras, Greece (in Greek)
16. Nurchi A, Valdes M (2005) Strengthening of stone masonry columns by means of cement-based composite wrapping. In: Hamelin P (ed) CCC 2005: 3rd international conference on composites in construction. Lyon, France, July 2005, pp 1189–1196
17. EN 1015-11 (1993) Methods of test for mortar for masonry – Part 11: determination of flexural and compressive strength of hardened mortar. European Committee for Standardization, Brussels